Comput. Methods Appl. Mech. Engrg. 209–212 (2012) 115–128

Contents lists available at SciVerse ScienceDirect

Comput. Methods Appl. Mech. Engrg.

journal homepage: www.elsevier.com/locate/cma

Three-dimensional mortar-based frictional contact treatment in isogeometric analysis with NURBS

İ. Temizer [a,*], P. Wriggers [b], T.J.R. Hughes [c]

[a] Department of Mechanical Engineering, Bilkent University, 06800 Ankara, Turkey
[b] Institute of Continuum Mechanics, Leibniz University of Hannover, Appelstr. 11, 30167 Hannover, Germany
[c] Institute for Computational Engineering and Sciences, The University of Texas at Austin, 201 East 24th Street, 1 University Station C0200, Austin, TX 78712-0027, United States

ARTICLE INFO

Article history:
Received 2 June 2011
Received in revised form 18 October 2011
Accepted 21 October 2011
Available online 2 November 2011

Keywords:
Three-dimensional contact
Isogeometric analysis
Mortar method
Friction

ABSTRACT

A three-dimensional mortar-based frictional contact treatment in isogeometric analysis with NURBS is presented in the finite deformation regime. Within a setting where the NURBS discretization of the contact surface is inherited directly from the NURBS discretization of the volume, the contact integrals are evaluated through a mortar approach where the geometrical and frictional contact constraints are treated through a projection to control point quantities. The formulation delivers a non-negative pressure distribution and minimally oscillatory local contact interactions with respect to alternative Lagrange discretizations independent of the discretization order. These enable the achievement of improved smoothness in global contact forces and moments through higher-order geometrical descriptions. It is concluded that the presented mortar-based approach serves as a common basis for treating isogeometric contact problems with varying orders of discretization throughout the contact surface and the volume.

1. Introduction

Non-smooth, mostly C^0-continuous, finite element discretization techniques constitute the most widely utilized approach in computational contact mechanics. It has been long recognized that such non-smoothness leads not only to convergence problems in iterative solution techniques but also to highly oscillatory *global contact interactions* such as tangential forces and rotation moments even when convergence is achieved. In order to alleviate some of these undesirable observations, various *geometrical smoothing* techniques have been developed based on Hermite, Bézier and NURBS descriptions [18,12,19,61,20,42,62,35,56,39,36]. Therein, the procedures operate on the contact surface only, leaving the bulk descriptions of the interacting solids away from the contact zone unchanged. Although surface smoothing leads to a considerable improvement of the contact force evolution, oscillations were observed to remain due to the strong interactions of the volume and surface discretizations, in particular at large deformations.

On the other hand, the robustness of contact computations also depends on an accurate and smooth description of not only the global but also the *local contact interactions*, i.e. the contact pressure and the tangential tractions. Mortar-based approaches constitute a method of consistently treating the contact interaction through an exact evaluation of the surface integrals contributing to the weak formulation, combined with a discrete satisfaction of the continuous contact constraints through projected quantities [54,22,49,25,13,50,48,21,26,59]. Such methods can be pursued in a purely penalty setting, possibly with Uzawa augmentations, in a Lagrange multiplier setting, or through an augmented Lagrangian approach [46]. For details and extensive references, the reader is referred to Wriggers [60], Laursen [37], Laursen et al. [38]. Mortar methods typically additionally deliver global *algorithmic smoothing* effects through particular choices of projection formulations, such as by defining nodally-averaged normals, but do not entirely eliminate the inherently geometrical effects. Moreover, it appears that a combined *global–local approach*, i.e. a surface smoothing technique combined with a mortar-based contact formulation, has not been explicitly investigated in the literature.

A natural departure point to achieve a smooth surface description which can then be combined with mortar-based approaches is an ideally exact characterization of the initial analysis geometry. The need to combine exact geometrical descriptions with contact constraints may arise in attempting to achieve convenient and theoretically robust parametrizations [33,34] or in attempting to virtually manipulate such exact descriptions in the presence of contact constraints [41,6]. Isogeometric analysis [27,9] is a computational mechanics technology which uses basis functions emanating from computer aided geometric design, such as B-Splines, NURBS, T-splines or subdivision surfaces instead of traditional C^0-continuous Lagrange finite element interpolatory polynomials

* Corresponding author. Tel.: +90 312 290 3064.
E-mail address: temizer@bilkent.edu.tr (İ. Temizer).

0045-7825/$ - see front matter © 2011 Elsevier B.V. All rights reserved.
doi:10.1016/j.cma.2011.10.014

and provides a general framework towards this purpose. Extensive investigations including fluid–solid interaction [3,2], the extended finite element method [5] and electromagnetics [8] have additionally demonstrated the ability of isogeometric analysis to provide not only more precise geometric representations than traditional finite elements but also efficient approaches to problems such as phase-field descriptions [16,17] and rotationless thin shell formulations [31,4]. These advantages are complemented by recent developments that allow a local refinement of the geometry description and consequently of the solution space through T-splines [11,52,53] – see also Borden et al. [7] for an application.

In the original work which introduced isogeometric analysis [27], it was suggested that smooth, compactly-supported basis functions might improve the modeling of contact problems. With a view towards this goal, a systematic mortar-based study of contact problems with isogeometric analysis was initiated in Temizer et al. [58] using NURBS discretizations. Qualitatively accurate satisfaction of thermomechanical frictionless contact constraints was observed even at coarse resolutions in two and three dimensions. Moreover, the pressure distributions in the classical Hertz contact problem were considerably smoother than those arising from Lagrange discretizations. In particular, the oscillations that were reported for the Hertz problem in Konyukhov and Schweizerhof [32] and subsequently in Franke et al. [15] for higher-order Lagrange discretizations were significantly alleviated with NURBS discretizations. These efforts were simultaneously paralleled by the approach reported in Lu [40] in a frictionless setting through alternative robust contact treatments based on the works of Papadopoulos and co-workers [30,43,55]. Subsequently, a two-dimensional mortar-based approach with friction was investigated in De Lorenzis et al. [10] where higher-order NURBS discretizations were observed to deliver smoother global interactions while ensuring the local quality of the solution.

The present work is an extension of the recent developments in Temizer et al. [58], De Lorenzis et al. [10]. The central contribution is a three-dimensional mortar-based frictional contact treatment in isogeometric analysis with NURBS in the finite deformation regime. For this purpose, in Section 2 the continuum contact problem is summarized and subsequently a mortar-based approach for treating geometrical and frictional contact constraints is introduced. Section 3 introduces the finite element description of the surface geometry where a contact NURBS patch is directly inherited from the volume NURBS patch without introducing an additional surface smoothing technique and thereby preserving the consistency between the volume and surface discretizations. Possible approaches to enforcing contact constraints are additionally discussed, among which projection to control point values in a mortar setting appears as the natural choice. Extensive numerical investigations are carried out in Section 4 in three main categories of typical benchmark problems where (i) the high quality of the local contact traction distributions are demonstrated for the contact of a deformable body with a rigid surface, followed by (ii) investigations where global contact variables such as forces and moments are monitored in the contact of two deformable bodies and it is shown that higher-order continuity on the surface as well as in the volume is necessary for arbitrarily smooth interactions, concluding by (iii) an industrially relevant example where the rolling of a Grosch-wheel is analyzed. The results support and extend the observations in Temizer et al. [58], De Lorenzis et al. [10] with particular discussions on the guaranteed non-negativity of the pressure distributions and the minimally oscillatory contact interactions with respect to alternative Lagrange discretizations independent of the order of the discretization. These findings reinforce the advantageous conclusion that the presented mortar-based approach serves as a common basis for treating isogeometric contact analysis problems with varying orders of discretization throughout the contact surface and the volume.

2. Contact treatment

2.1. Continuum contact mechanics formulation

The emphasis of this work is on purely mechanical finite deformation quasi-static frictional contact problems. Denoting the reference and current configurations of a body $\mathcal{B}$ via $\mathcal{R}_o$ and $\mathcal{R}$, related to each other by the motion $\boldsymbol{x}=\boldsymbol{\chi}(\boldsymbol{X})$ that induces $\boldsymbol{F}=\mathrm{Grad}[\boldsymbol{x}]$, the strong form of the linear momentum balance in referential form is

$$\mathrm{Div}[\boldsymbol{P}]=\boldsymbol{0} \quad \text{in} \quad \mathcal{R}_o \tag{2.1}$$

with the associated traction $\boldsymbol{p}=\boldsymbol{P}\boldsymbol{N}$. On the non-overlapping portions of the boundary $\partial\mathcal{R}_o=\partial\mathcal{R}_o^x\cup\partial\mathcal{R}_o^p\cup\partial\mathcal{R}_o^c$, the boundary conditions

$$\boldsymbol{x}=\hat{\boldsymbol{x}} \quad \text{on} \quad \partial\mathcal{R}_o^x \quad \text{and} \quad \boldsymbol{p}=\hat{\boldsymbol{p}} \quad \text{on} \quad \partial\mathcal{R}_o^p \tag{2.2}$$

are prescribed where $\hat{\boldsymbol{p}}$ is assumed to be deformation-independent.

The contact between two bodies $\mathcal{B}^{(1)}$ and $\mathcal{B}^{(2)}$ will eventually be treated within a master/slave (or, mortar/non-mortar) setting where $\mathcal{B}^{(1)}$ is the slave (non-mortar) side. In the continuum formulation, the matching contact interface $\partial\mathcal{R}^c:=\partial\mathcal{R}^{(1),c}=\partial\mathcal{R}^{(2),c}$ on the deformed configuration is pulled back to $\partial\mathcal{R}_o^c:=\partial\mathcal{R}_o^{(1),c}\neq\partial\mathcal{R}_o^{(2),c}$. All contact integrals are subsequently evaluated on $\partial\mathcal{R}_o^c$. The weak form of the balance equation is then expressed as

$$\begin{aligned}\delta\mathcal{G}:=&-\sum_{I=1}^{2}\int_{\mathcal{R}_o^{(I)}}\delta\boldsymbol{F}\cdot\boldsymbol{P}\,\mathrm{d}V+\sum_{I=1}^{2}\int_{\partial\mathcal{R}_o^{(I),p}}\delta\boldsymbol{x}\cdot\hat{\boldsymbol{p}}\,\mathrm{d}A\\&+\int_{\partial\mathcal{R}_o^c}(\delta\boldsymbol{x}^{(1)}-\delta\boldsymbol{x}^{(2)})\cdot\boldsymbol{p}\,\mathrm{d}A=0\end{aligned} \tag{2.3}$$

where $\boldsymbol{p}:=\boldsymbol{p}^{(1)}$. The contact traction is decomposed as $\boldsymbol{p}=p_N\boldsymbol{v}-\boldsymbol{\tau}$ where $\boldsymbol{v}$ is the outward unit normal to $\partial\mathcal{R}_o^{(2),c}$. Using the standard definition $g_N=-(\boldsymbol{x}^{(1)}-\boldsymbol{x}^{(2)})\cdot\boldsymbol{v}$ for the normal gap, the contact contribution to the weak form can be expressed as

$$\delta\mathcal{C}:=\int_{\partial\mathcal{R}_o^c}(\delta\boldsymbol{x}^{(1)}-\delta\boldsymbol{x}^{(2)})\cdot\boldsymbol{p}\,\mathrm{d}A=-\int_{\partial\mathcal{R}_o^c}(\delta g_N\,p_N+\delta\xi^\alpha\tau_\alpha)\,\mathrm{d}A \tag{2.4}$$

under the standard assumption of an exact satisfaction of the impenetrability condition $g_N=0$ to simplify the tangential contribution with ξ^α as the convected curvilinear coordinates on the master surface and τ_α as the covariant components of the tangential traction. All contact variables are evaluated through the closest point projection of a slave (integration) point to the master surface.

Karush–Kuhn–Tucker conditions for impenetrability constraints on $\partial\mathcal{R}^c$ are

$$g_N\leqslant 0,\quad p_N\geqslant 0,\quad g_N\,p_N=0. \tag{2.5}$$

For the tangential contribution, the Coulomb slip criterion

$$\Phi(\boldsymbol{\tau},p_N):=\|\boldsymbol{\tau}\|-\mu\,p_N\leqslant 0 \tag{2.6}$$

is assumed where $\|\boldsymbol{\tau}\|^2=\tau^\alpha\tau_\alpha$. Here and in the following, standard notation associated with surface parametrization is employed: e.g. $\boldsymbol{a}_\alpha:=\frac{\partial\boldsymbol{x}^{(2)}}{\partial\xi^\alpha}$ are the covariant basis vectors on the master surface which define the covariant metric components $a_{\alpha\beta}:=\boldsymbol{a}_\alpha\cdot\boldsymbol{a}_\beta$ whose inverse delivers the contravariant metric components $a^{\alpha\beta}$ such that $\tau^\alpha=a^{\alpha\beta}\tau_\beta$. During slip, the evolution law for the projection coordinates is

$$\dot{\xi}^\alpha=\dot{\lambda}\frac{\tau^\alpha}{\|\boldsymbol{\tau}\|} \tag{2.7}$$

with which the tangential constraints can be stated as

$$\Phi\leqslant 0,\quad \dot{\lambda}\geqslant 0,\quad \Phi\,\dot{\lambda}=0. \tag{2.8}$$

For details and extensive references on computational contact mechanics, the reader is referred to the monographs Laursen [37], Wriggers [60].

2.2. Mortar-based finite element discretization

The variations δg_N and $\delta\xi^\alpha$ appearing in $\delta\mathcal{C}$ are purely kinematic in nature. A contact treatment based on the mortar method defines the evolution of the kinetic quantities p_N and τ_α such that well-defined pressure and frictional traction distributions are obtained which satisfy the contact patch tests, in comparison to e.g. the node-to-surface algorithms, while numerical robustness and smoothly varying reaction forces that do not display surface locking are ensured, in comparison to e.g. a point-wise enforcement of the contact constraints [44].

While mortar-based contact treatment has been extensively investigated, the studies have predominantly been restricted to linear and quadratic surface elements in the two-dimensional setting and to bilinear/biquadratic quadrilateral and triangular surface elements in three dimensions – see Section 1 for references. In the context of isogeometric analysis, a primary goal is to treat all orders of discretization through a single unified numerical framework. In particular, segmentation of the contact interface for exact numerical integration appears to be impractical for arbitrary discretizations which may arise in geometrical modeling and therefore will not be pursued. Consequently, the present study builds on the mortar studies of linear elements and presents a formulation that is subsequently applied without modification in all analyses. While this choice may not be the most appropriate one from a mathematical point of view, in particular for Lagrange basis functions, it is highlighted that preserving flexibility in a unified treatment of geometrical design and computational contact analysis is of primary interest in the present work. In a two-dimensional setting, this approach has already proved satisfactory as extensively demonstrated with frictionless contact in Temizer et al. [58] as well as in the presence of friction in De Lorenzis et al. [10]. Therefore, all mortar integrals are evaluated through integration on the slave surface NURBS elements by evaluating the contact variables at the closest point projection of the integration point to the master surface. The order of integration is chosen to be sufficiently high in order to minimize the error in the evaluation of the integrals, following Fischer and Wriggers [13,14].

The presently employed mortar method closely follows earlier works based on a penalty regularization of the contact constraints supplemented by Uzawa augmentations. The formulation is consistently linearized and implemented within an iterative Newton–Raphson procedure to achieve quadratic convergence.

2.2.1. Normal contribution

The slave surface is the integration domain for the weak form of the contact contribution. On this surface, the discretization $\boldsymbol{x}^{(1)} := \sum_I R^I \boldsymbol{x}^{(1),I}$ is employed while the master surface admits the discretization $\boldsymbol{x}^{(2)} := \sum_J Q^J \boldsymbol{x}^{(2),J}$. In general, these disretizations are not interpolatory and the basis functions $\{R^I, Q^J\}$ are rational polynomials in the context of NURBS – see Section 3. The key ingredient of a mortar-based method is the projection of kinematic quantities to degrees of freedom. Using the notation $\langle\mathcal{Q}\rangle := \int_{\partial\mathcal{R}_0^\xi} \mathcal{Q}\,\mathrm{d}A$ for a generic quantity $\mathcal{Q}$, the projection

$$\bar{g}_N^I := \langle R^I g_N\rangle \tag{2.9}$$

for the normal part defines a regularized projected contact pressure (ϵ_N: normal penalty parameter)

$$\bar{p}_N^I = \epsilon_N \bar{g}_N^I. \tag{2.10}$$

Note that it is not necessary to associate a unique normal with each projection in the present formulation since the surface normal information essentially appears in the projection integral – cf. Puso and Laursen [49]. In a Lagrange multiplier setting, the contact constraints would be satisfied by the projected quantities which determine the active set:

$$\bar{g}_N^I \leqslant 0, \quad \bar{p}_N^I \geqslant 0, \quad \bar{g}_N^I\,\bar{p}_N^I = 0. \tag{2.11}$$

Algorithmically, the detection of contact/separation to update the active set $\mathcal{A}$ is carried out via

$$\text{Contact Status Update for } I: \begin{cases} I \notin \mathcal{A} & \text{then} \begin{cases} \bar{g}_N^I > 0 & \to I \in \mathcal{A} \\ \text{else} & \to I \notin \mathcal{A} \end{cases} \\ I \in \mathcal{A} & \text{then} \begin{cases} \bar{p}_N^I \leqslant 0 & \to I \notin \mathcal{A} \\ \text{else} & \to I \in \mathcal{A} \end{cases} \end{cases} \tag{2.12}$$

It is remarked that since (2.11) replaces (2.5), $g_N > 0$ or $p_N < 0$ is possible – see Section 4.2.

The local pressure is defined via a discretization as for all other degrees of freedom on the slave surface via

$$p_N = \sum_I R^I p_N^I \tag{2.13}$$

where the following discrete quantities are defined:

$$g_N^I := \frac{\bar{g}_N^I}{\langle R^I\rangle} \quad \to \quad p_N^I := \frac{\bar{p}_N^I}{\langle R^I\rangle} \equiv \epsilon_N g_N^I. \tag{2.14}$$

While the penalty regularization alone allows active set update by monitoring $\bar{g}_N^I$ only, Uzawa augmentations will be pursued in the next section such that the Lagrange multiplier solution is approximately captured. For this reason, the active set update still follows algorithm (2.12).

The contact constraints are, in general, not satisfied by g_N^I and p_N^I in a Lagrange multiplier setting [22,59], presently since the normalizing term $\langle R^I\rangle$ may be negative. This occurs in the case of Lagrange elements of order greater than one. NURBS basis functions, however, are non-negative pointwise and therefore the constraints may be stated in terms of either the projected or the discrete quantities.

2.2.2. Tangential contribution

For the regularized treatment of the tangential part within the standard framework where a stick predictor step is followed by slip correction, the primary quantities employed are the projected quantities. Since the emphasis of this work is on the use of NURBS basis functions which are guaranteed to be non-negative, the final formulation is presented in the following simplified version. In the predictor step, a discrete incremental slip is defined[1]:

$$\Delta\xi^{\alpha,I} := \frac{\langle R^I \Delta\xi^\alpha\rangle}{\langle R^I\rangle}. \tag{2.15}$$

This definition delivers a trial update, for active set members $\{I,J\}$,

$$\tau_\alpha^{I,n+1,tr} = \tau_\alpha^{I,n} + \epsilon_T \sum_J a_{\alpha\beta}^{IJ} \Delta\xi^{\beta J} \tag{2.16}$$

to the discrete contact traction component along each curvilinear coordinate at a given Newton–Raphson iteration at the $(n+1)$th load step. Here, ϵ_T is the tangential penalty parameter and

$$a_{\alpha\beta}^{IJ} := \frac{\langle R^I a_{\alpha\beta} R^J\rangle}{\langle R^I\rangle\langle R^J\rangle} \tag{2.17}$$

is a discrete covariant metric. The metric is non-zero only for degrees of freedom $\{I,J\}$ which belong to the same element and hence

[1] The notation $\Delta(\bullet)$ should not be confused with the linearization notation. Linearization is not treated here.

the implementation of Eq. (2.16) does not cause a significant computational expense compared to alternative formulations.

The predictor step is followed by a check for slip

$$\|\boldsymbol{\tau}^{I,n+1,tr}\| - \mu\, \bar{p}_N^I \leqslant 0 \tag{2.18}$$

where, using discrete contravariant metric components $m^{\alpha\beta,IJ}$ which are defined by the inverse components of $m_{\alpha\beta}^{IJ}$ with respect to α and β,

$$m_{\alpha\beta}^{IJ} = \frac{a_{\alpha\beta}^{IJ}}{\langle R^I R^J \rangle} \quad \rightarrow \quad \|\boldsymbol{\tau}^{I,n+1,tr}\|^2 := \tau_\alpha^{I,n+1,tr} m^{\alpha\beta,IJ} \tau_\beta^{I,n+1,tr}. \tag{2.19}$$

If the slip criterion is not violated, $\tau_\alpha^{I,n+1} = \tau_\alpha^{I,n+1,tr}$. Otherwise,

$$s_\alpha^I := \frac{\tau_\alpha^{I,n+1,tr}}{\|\boldsymbol{\tau}^{I,n+1,tr}\|} \quad \rightarrow \quad \tau_\alpha^{I,n+1} = \mu \bar{p}_N^I s_\alpha^I. \tag{2.20}$$

For numerical robustness and accuracy, the penalty regularization is complemented by Uzawa augmentations which update the normal and tangential tractions to convergence at each load step – see also Section 4.1. For this purpose, the replacements $\tau_\alpha^{I,n} \leftarrow \tau_\alpha^{I,(k)}$ and $\tau_\alpha^{I,n+1,tr} \leftarrow \tau_\alpha^{I,(k+1),tr}$ are substituted in the update (2.16) where k indexes the Uzawa augmentations at the $(n+1)$th load step. Subsequently, the same predictor–corrector scheme is pursued for the augmented tangential tractions. The augmentation for the normal contribution reads

$$p_N^{I,(k+1)} = p_N^{I,(k)} + \epsilon_N g_N^{I,(k+1)}. \tag{2.21}$$

Subsequently, using Eq. (2.14), $\bar{p}_N^{I,(k+1)} = p_N^{I,(k+1)} \langle R^I \rangle$ is employed to check for contact loss. The active set is updated before the augmentation of the tangential tractions in order to ensure the consistency of the updated tangential tractions with respect to the slip criterion employing the augmented pressures.

The details of the complete mortar formulation, together with its variational basis in a more general context and comparisons with alternative approaches, will be presented elsewhere [57].

3. Isogeometric treatment with NURBS

3.1. Geometric description

The central ingredient of an isogeometric contact treatment is to pursue a NURBS discretization of the contact surface that is inherited in a straightforward fashion from the NURBS discretization of the volume [58]. In contrast to earlier surface smoothing techniques, this approach directly delivers a consistent treatment of volumetric and contact analysis. The NURBS-based isogeometric discretization is briefly recalled here only for the contact surface description. The reader is referred to Piegl and Tiller [45] and Cottrell et al. [9] for further details and extensive references.

Along each surface coordinate ξ^α, an open non-uniform knot vector

$$\Xi^\alpha = \left\{ \underbrace{\xi_0^\alpha, \ldots, \xi_{p_\alpha}^\alpha}_{p_\alpha+1 \text{ equal terms}}, \xi_{p_\alpha+1}^\alpha, \ldots, \xi_{n_\alpha}^\alpha, \underbrace{\xi_{n_\alpha+1}^\alpha, \ldots, \xi_{m_\alpha}^\alpha}_{p_\alpha+1 \text{ equal terms}} \right\} \tag{3.1}$$

is constructed for the geometric description where $m_\alpha = n_\alpha + p_\alpha + 1$, p_α is the polynomial order of the accompanying B-spline basis functions, ξ_j^α is the jth knot and $n_\alpha + 1$ would be the number of accompanying control points in a one-dimensional setting. Using a Ξ^1 and a Ξ^2, the rational B-spline (NURBS) basis functions $R_{d_1 d_2} \geqslant 0$ are defined as

$$R_{d_1 d_2}(\xi^1, \xi^2) = \frac{w_{d_1 d_2}}{W(\xi^1, \xi^2)} B_{d_1}^1(\xi^1)\, B_{d_2}^2(\xi^2) \tag{3.2}$$

with $B_{d_\alpha}^\alpha$ as a nonrational B-spline basis function. The normalizing weight W is given in terms of the weights $w_{d_1 d_2} > 0$ and $B_{d_\alpha}^\alpha$ via

$$W(\xi^1, \xi^2) = \sum_{d_1=0}^{n_1} \sum_{d_2=0}^{n_2} w_{d_1 d_2} B_{d_1}^1(\xi^1)\, B_{d_2}^2(\xi^2). \tag{3.3}$$

The contact surface is then parametrized by

$$\boldsymbol{S}(\xi^1, \xi^2) = \sum_{d_1=0}^{n_1} \sum_{d_2=0}^{n_2} R_{d_1 d_2}(\xi^1, \xi^2) \boldsymbol{P}_{d_1 d_2} \tag{3.4}$$

where $\boldsymbol{P}_{d_1 d_2}$ are the control points. All the geometry information is inherited from the volume by evaluating its parametrization on the contact surfaces [58]. The knot vectors together with the associated control points and the accompanying weights constitute a *contact patch*.

In the finite element setting, all degrees of freedom are discretized via the same NURBS basis functions that are used for the geometric description, including the discretized mortar quantity p_N. In the following sections, the order of the NURBS parametrization will be denoted by $\mathcal{N}^p$, while the order of Lagrange polynomials employed will be denoted by $\mathcal{L}^p$. It is noted that, in order to obtain a refined volume parametrization from which the contact surface parametrization is inherited, the *k-refinement* procedure is employed where order elevation precedes knot refinement [9]. In this setting, a NURBS volume/contact *element* corresponds to a region bounded by unique knot entries and acts as a convenient integration domain.

The implementation of frictional contact with two deformable bodies demands the calculation of the derivatives of the basis functions up to order three. First derivatives are standard and already necessary for the volumetric analysis. An explicit expression for the second-order derivatives which are required for the linearization of δg_N has been provided in Temizer et al. [58]. The third-order derivatives required for the linearization of $\delta \xi^\alpha$ can be obtained in a similar fashion.

3.2. Enforcing contact constraints

In order to enforce the normal and tangential contact constraints in the context of isogeometric analysis, several possible algorithms are briefly reviewed below.

1. *Collocation at Unique Knot Entries:* Constraints may be enforced by a (point) collocation approach at the physical points associated with the unique knot entries, which also form the vertices of the isogeometric contact elements, in the same spirit as the classical node-to-surface (NTS) algorithm. The transfer of frictional history variables and the augmentations would also be associated with these collocation points. However, in general, the number of unique knot entries is less than the number of degrees of freedom which describe the contact surface. In other words, in the context of a simple example, the pointwise penetration of a NURBS surface with a rigid one may be varied by moving the control points while simultaneously satisfying such constraints. Consequently, one would obtain an underconstrained formulation (with respect to the mortar-KTS algorithm).
2. *KTS Algorithm:* A direct integration of the contact contribution (2.4) to the weak form by enforcing the constraints at the physical points of the quadrature points (which can be associated with virtual knots) leads to a straightforward scheme which has the advantage that the contact surface can be qualitatively satisfactorily captured even with a low number of elements, contrary to all other possibilities. This approach was called the *knot-to-surface (KTS) algorithm* in Temizer et al. [58] and was demonstrated for finite deformation thermomechanical contact problems without friction. Also shown in this work was that this approach is overconstrained and therefore not

acceptable if a robust formulation with accurate tractions is desired – a fact that is well-known from standard contact elements. These observations were further demonstrated in the two-dimensional frictional isogeometric setting in De Lorenzis et al. [10].

3. *Collocation at Special Abscissae:* The direct analog of the classical NTS algorithm in an isogeometric setting requires the same number of collocation points as the unknowns. One such possible option might be to employ the physical points associated with Greville abscissae of the knot vector [29]. See Politis et al. [47] for an application to isogeometric analysis in the context of the boundary element method and Aurrichio et al. [1] for further applications in addition to the use of Demko abscissae. Such possibilities are not investigated in this work since they would carry the known disadvantages of the NTS algorithm to the isogeometric setting. Nevertheless, these might potentially be more practical and time-efficient in situations, such as impact problems, where the additional cost associated with the evaluation of mortar integrals could be unacceptable. Within this algorithm, the constraints would be checked and the augmentations would be conducted as in algorithm 1.
4. *Mortar-KTS Algorithm:* The approach that combines the robust mortar-based contact treatment with isogeometric analysis is the *mortar-KTS* algorithm [58]. Similar to the KTS algorithm, this is not a collocation approach since the weak form of the contact constraints is evaluated exactly via integration. However, in a frictionless setting, a mortar projection to *control pressures* (p_N^l) is employed to obtain the correct number of constraints. In the frictional setting, a mortar projection for both normal and tangential control tractions is employed [10]. It is highlighted that the projected normal gap $\bar{g}_N^l = \langle R^l g_N \rangle$, or more appropriately g_N^l for the correct dimension, is not associated with the physical normal gap corresponding to the control point I in general. Now, since this gap is enforced to zero by the formulation, one could pursue elementary arguments, e.g. through the mean value theorem for integrals, to conclude that there exists a knot value in [0,1], say $\xi^{\alpha,I}$, in the span of R^I such that the normal gap of its physical point is zero. A similar argument applies to the tangential (elastic) gaps. Overall, there is a correct number of such points – cf. collocation at special abscissae. However, these knot values would evolve with the solution and therefore are not of practical use in enforcing the constraints, which would make the algorithm an equivalent of the NTS-type approach. It is sufficient and more practical to track the control values.

In view of its demonstrated advantages, the approach that is employed in this work is algorithm 4 in the context of the mortar treatment summarized in Section 2.2. A full investigation of algorithms 1 and 3 as well as their comparison with the present choice remains an issue open to further investigation.

4. Numerical investigations

In this section, various aspects of the introduced mortar-based algorithm will be demonstrated in the finite deformation regime with rigid and deformable master bodies. Although three-dimensional mortar-based frictionless contact using NURBS basis functions has not been explicitly treated earlier, all of the examples presented will include friction. However, some of the observations, such as the smoothness in the contact pressure distribution, could also be shown without friction.

The investigations are grouped into three major categories based on various standard benchmark problems of computational contact mechanics. In Section 4.2, the local quality of the solution, namely the pressure and the tangential traction distributions, is demonstrated. The global quality of the solution is analyzed in Section 4.3 with a large rotational sliding problem and in Section 4.4 with a large tangential sliding one. Finally, an industrially relevant case is considered in Section 4.5 in the context of a rolling Grosch wheel.

4.1. Modeling and discretization parameters

For the bulk modeling, a classical Neo-Hookean type material model with volumetric-deviatoric decoupling will be employed based on the strain energy function ($J = \det[\boldsymbol{F}]$ and $\boldsymbol{C} = \boldsymbol{F}^T\boldsymbol{F}$)

$$\mathcal{W} = \frac{\Lambda_1}{2}(\ln J)^2 + \frac{\Lambda_2}{2}(J^{-2/3}\mathrm{tr}[\boldsymbol{C}] - 3). \tag{4.1}$$

In all of the investigations, the bulk and shear moduli $\{\Lambda_1, \Lambda_2\}$ correspond to the choices of a Young's modulus $E = 10$ and a Poisson's ratio $\nu = 0.3$.

For the contact computations, the friction coefficient is set to $\mu = 0.3$ unless otherwise noted. The base values of the penalty parameters in all computations are $\epsilon_N = 100$ and $\epsilon_T = 10$ which are multiplied by the largest diagonal entry of the volumetric stiffness matrix associated with the deformable bodies at the first Newton–Raphson iteration of the first Uzawa augmentation, but subsequently kept constant at this value through each load step, before being transferred to the contact computations. These choices already deliver a qualitatively satisfactory solution with a very small penetration even at large normal and tangential loads. Uzawa iterations additionally augment the multipliers to convergence to within a tolerance of TOL. Denoting the vector of all discrete augmentation variables $p_N^{I,(k+1)}$ and $\tau_\alpha^{I,(k+1)}$ (see Section 2.2.2) by $\{\lambda\}^{(k+1)}$, the criterion for convergence is

$$\frac{\|\{\lambda\}^{(k+1)} - \{\lambda\}^{(k)}\|}{\|\{\lambda\}^{(k)}\|} \leqslant \mathrm{TOL}. \tag{4.2}$$

The results with the given base values of ϵ_N and ϵ_T together with TOL = 0.01 are quantitatively in very good agreement with the case of TOL = 0.001, below which only negligible changes are observed in the solution if any. The larger tolerance is therefore chosen for numerical efficiency. An exact linearization of the presented mortar approach has been implemented to additionally ensure iterative efficiency.

It is recalled that the augmentation convergence is affected by the penalty parameters not only in terms of the number of iterations to convergence but also in terms of the final solution quality. For instance, alternative choices of $\epsilon_N = 10$ and $\epsilon_T = 1$ as base values deliver inferior results at TOL = 0.01 and the number of iterations is larger for a high quality solution that requires TOL = 0.001. On the other hand, too high a penalty parameter causes well-known convergence difficulties at large penetrations already without friction, as was recently further investigated in Zavarise et al. [63]. For this reason, all simulations in the present study have been run with a load step size adaptivity option. However, a step size reduction was needed only a few times overall for the simulations presented. Consequently, it can be stated that the simulations were very stable and in many instances larger load steps could be taken although this would now introduce an error due to the tangential traction component update.

Table 1
The default number of Gauss–Legendre integration points employed in each direction.

	$\mathcal{N}^2$	$\mathcal{N}^3$	$\mathcal{N}^4$	$\mathcal{L}^1$	$\mathcal{L}^2$	$\mathcal{L}^3$	$\mathcal{L}^4$
Volume element	4	6	6	2	4	4	6
Contact element	6	6	6	4	4	9	12

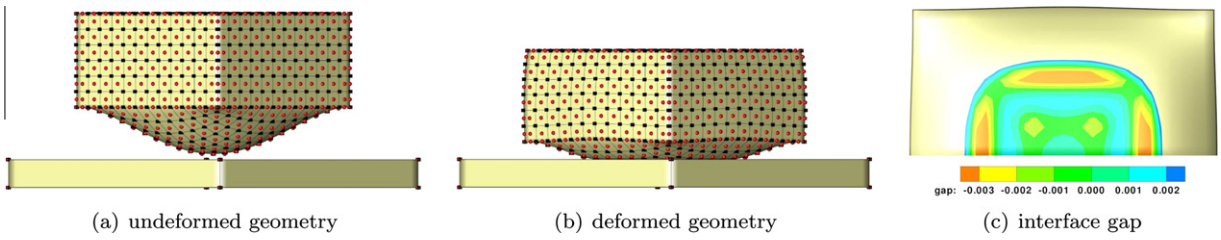

Fig. 1. An example solution to the contact traction quality investigation of Section 4.2 is shown based on an $\mathcal{N}^2$-discretization. In this and similar figures, the black squares indicate the physical positions of the unique knot entries and the red spheres denote the control point locations. In the interface gap plot, only half of the contact zone when viewed from below is shown. A representative dimension of the deformable body is the width $L_o = 1$. (For interpretation of the references to colour in this figure legend, the reader is referred to the web version of this article.)

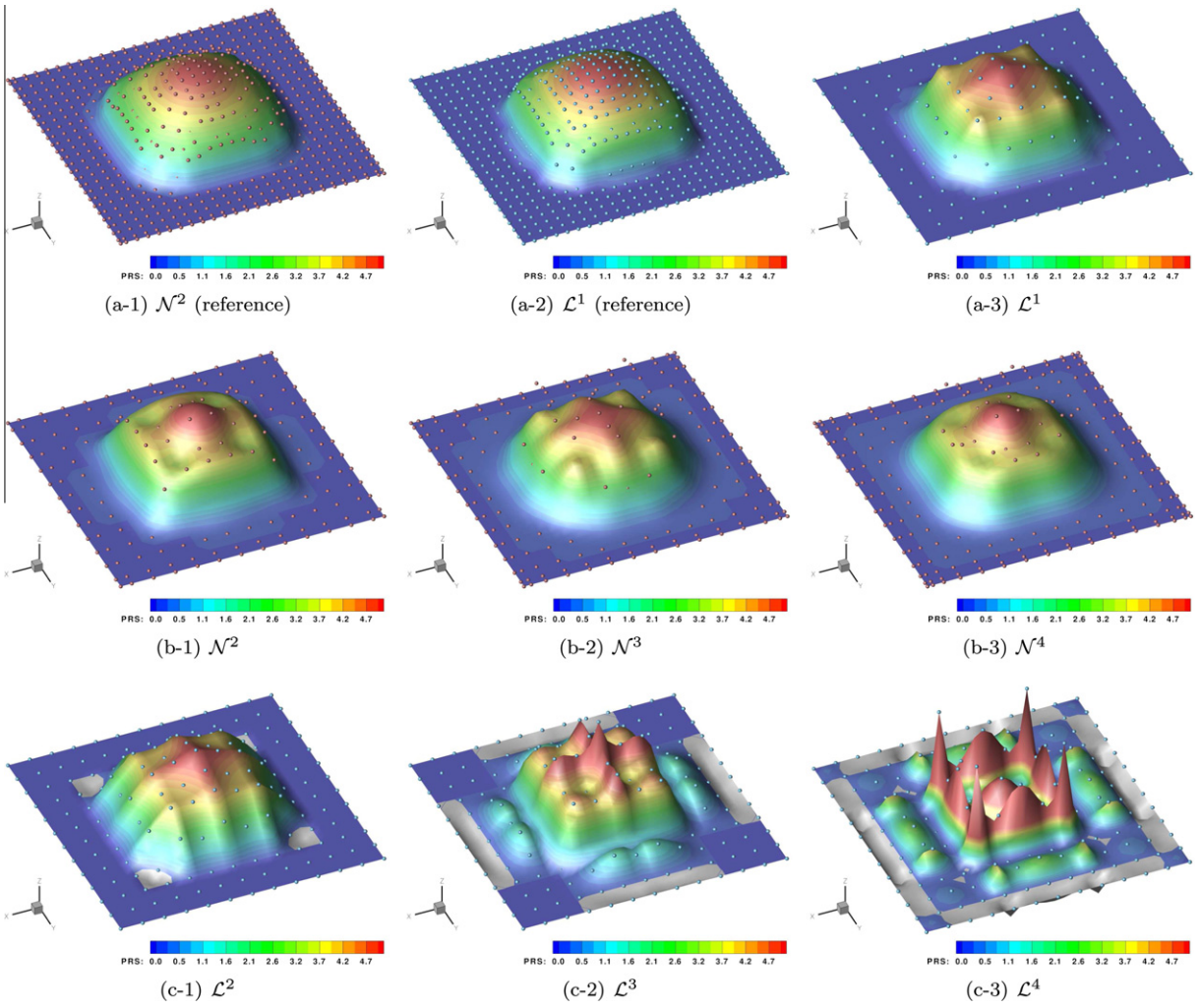

Fig. 2. Contact pressure $P_{RS} \equiv p_N$ distributions are shown for the problem described in Fig. 1 for NURBS ($\mathcal{N}^p$) and Lagrange ($\mathcal{L}^p$) basis functions of order p. The reference solutions are computed with the discretization shown therein. The gray areas in the $\mathcal{L}^p$-discretizations indicate negative pressure zones. The spheres correspond to p_N^I. The height of the points for $\mathcal{L}^4$ have been scaled by 0.4 in comparison to the other figures.

The order p of NURBS ($\mathcal{N}^p$) and Lagrange ($\mathcal{L}^p$) discretizations will be denoted explicitly in all examples. The default number of integration points employed for each discretization type along each direction is provided in Table 1. See Hughes et al. [28] for a recent discussion of efficient quadrature schemes appropriate for isogeometric analysis. Presently, a significantly increasing number with increasing order is chosen for $\mathcal{L}^p$-discretizations because the number of NURBS elements does not change during order elevation whereas it is reduced for Lagrange discretizations. The stated number of elements in the following investigations are valid for all $\mathcal{N}^p$ and $\mathcal{L}^1$. Only the discretization resolution and the order of the bodies in the plane of contact have been varied in the investigations. The discretization in the direction perpendicular to the plane of contact will be denoted explicitly and it has been verified that it does not influence the conclusions drawn.

4.2. Local quality: contact tractions

In the first example, where a deformable body is pressed onto a rigid surface under displacement control at the top surface at five

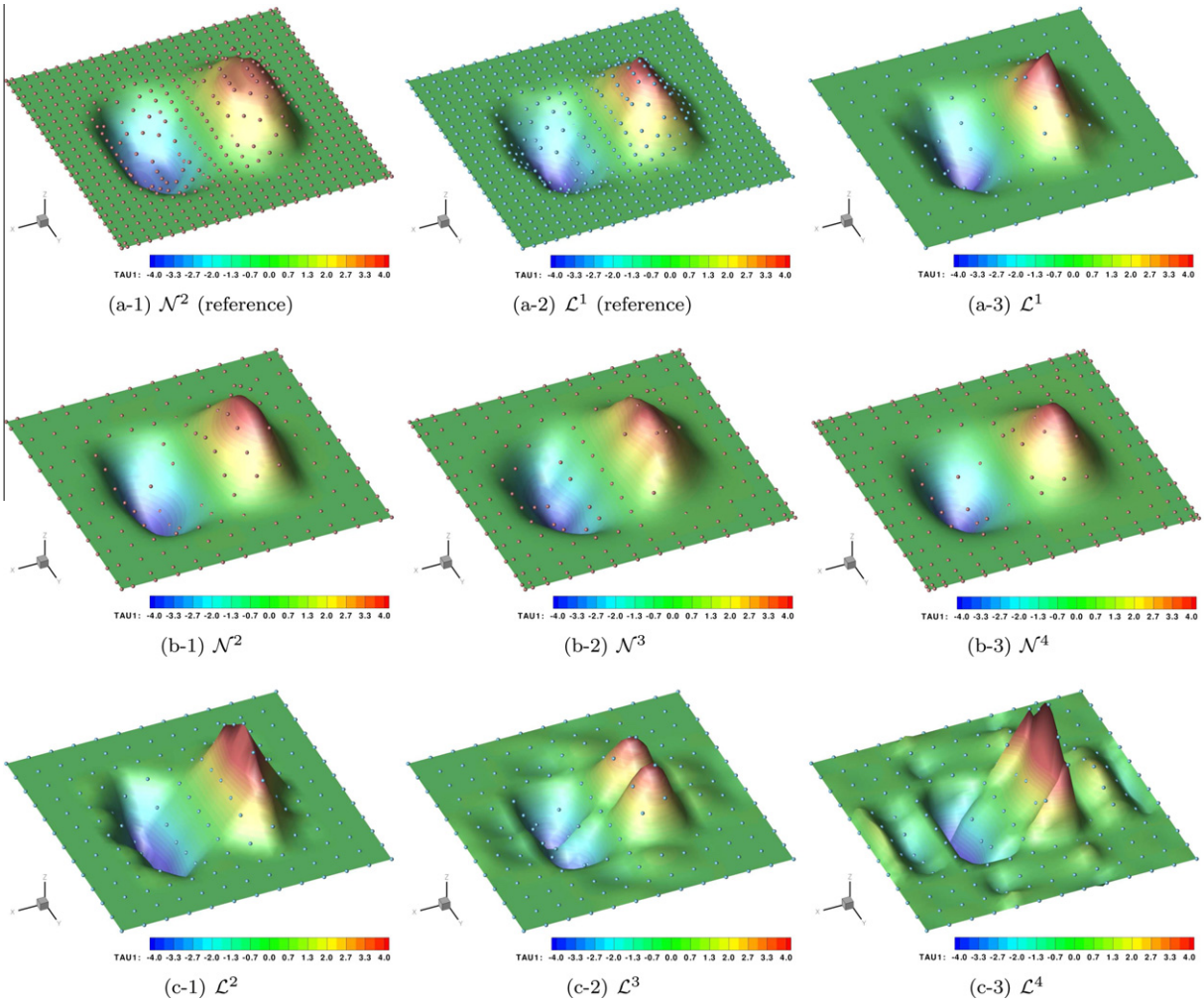

Fig. 3. The tangential traction component $\text{TAU1} \equiv \tau_1/\mu$ for the analysis of Fig. 2 is shown for NURBS ($\mathcal{N}^p$) and Lagrange ($\mathcal{L}^p$) basis functions of order p. The second component displays identical variations in the other direction. The spheres correspond to τ_1^l/μ.

load steps through 0.3 units, the local quality of the solution is investigated by monitoring the contact pressure p_N and the tangential traction component τ_1. The problem geometry is shown[2] in Fig. 1 discretized at a reference resolution with $\mathcal{N}^2$ where 24 elements are employed in each lateral direction. For the coarse resolution computations, 12 elements are employed in each lateral direction. In the vertical direction, 6 elements are employed together with an $\mathcal{N}^2$-discretization for $\mathcal{N}^p$ and an $\mathcal{L}^1$-discretization for $\mathcal{L}^p$ investigations. Fig. 1 also displays the gap distribution within the contact zone. In comparison to a representative dimension L_o of the deformable body, the gap magnitude is seen to be $\mathcal{O}(10^{-3}L_o)$ which additionally verifies the quantitative accuracy of the chosen augmentation tolerance. It has been verified that the changes in the results are negligible when the tolerance is decreased to $\text{TOL} = 0.001$.

The contact pressure distributions for various coarse discretizations are compared with reference $\mathcal{N}^2$ and $\mathcal{L}^1$ solutions in Fig. 2. Two major observations are that (i) $\mathcal{N}^p$-discretizations deliver a non-negative pressure distribution and (ii) increasing the order p does not deteriorate (in fact improves as to be demonstrated in the following sections) the quality of the solution where the distributions remain minimally oscillatory even at this coarse discretization although the span of each basis function moves well beyond the contact zone. The former observation is guaranteed through the employed mortar approach due to the non-negativeness of the NURBS basis functions – see Section 2.2.1. The latter observation is significant since it demonstrates that the summarized mortar-based contact treatment is *uniformly applicable* to all $\mathcal{N}^p$-discretizations while ensuring a reliable and robust solution. This is of critical importance since a major goal of isogeometric analysis is a unified treatment of design and analysis. From this point of view, it would not be advantageous to employ a modified special contact treatment technique for each order and clearly this is not necessary. In the case of $\mathcal{L}^p$-discretizations, neither observation holds. In particular, the oscillatory response at coarse discretizations has been observed earlier in various settings [32,15,58]. While a $p_N \geqslant 0$ requirement, although physically sound, may not be deemed critical and even restrictive since the contact constraints are satisfied only by the projected quantities, the need for an explicit treatment of higher-order $\mathcal{L}^p$-discretizations is clear and has been pursued mostly for the case of $\mathcal{L}^2$ [24,14,55,50]. Nevertheless, in all upcoming investigations a common treatment of all

[2] The exact geometrical description requires the complete knot vectors and weights. In the following, since slightly more or less deformation does not affect the conclusions drawn and the order of magnitude of the deformations are apparent in the figures, only representative dimensions of the problem and the boundary conditions are supplied.

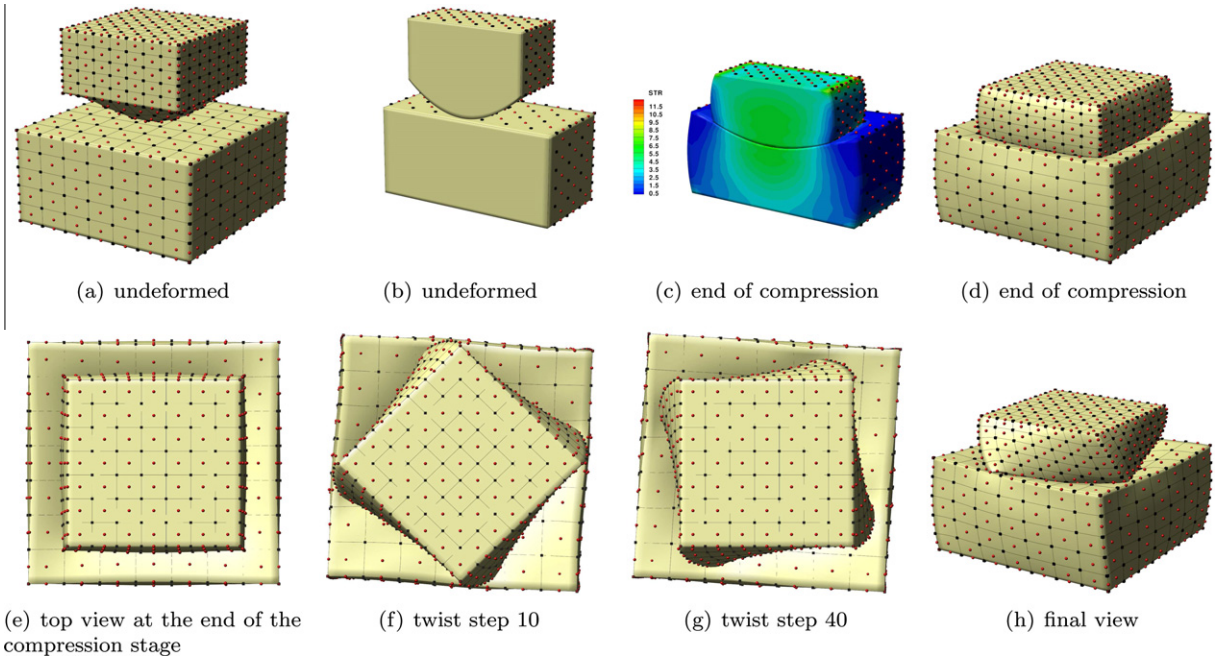

Fig. 4. Simulation instances from the investigation of Section 4.3 are shown at a fine $\mathcal{N}^2$-discretization with seven elements in each lateral direction and five in the vertical direction for both the slave and the master body. The large compressive and shear deformations are clearly observed. Here, $\text{STR} \equiv \|\boldsymbol{P}\|$. The lower (master) body has dimensions $1.5 \times 1.5 \times 0.75$ and the initial gap between the bodies is approximately 0.025 units.

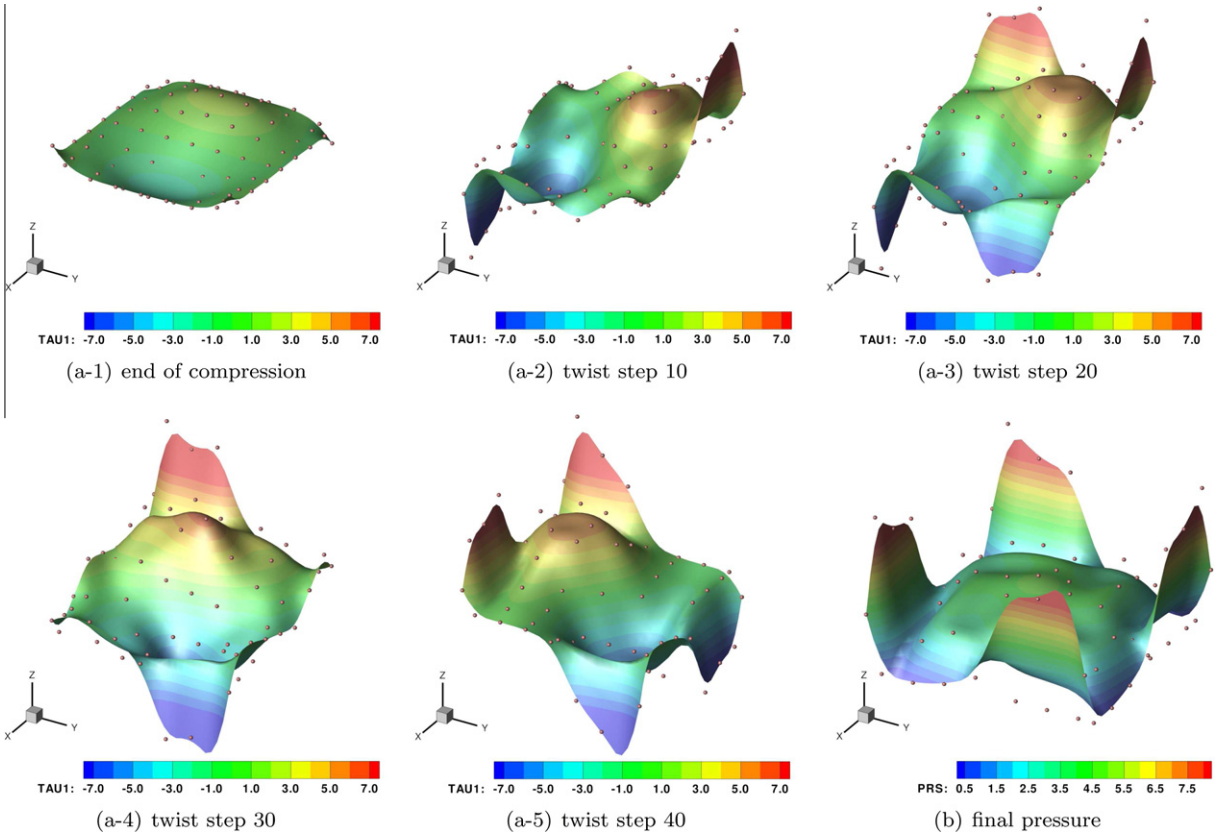

Fig. 5. The tangential traction component $\text{TAU1} \equiv \tau_1/\mu$ distribution evolution and the final pressure $\text{PRS} \equiv p_N$ distribution are shown for the problem of Fig. 4.

$\mathcal{L}^p$-discretizations will be pursued. It is remarked, however, that the goal of the present work is to demonstrate the uniformly high solution quality for the mortar-based $\mathcal{N}^p$-discretizations rather than highlight a need for improved $\mathcal{L}^p$-discretizations.

The uniformly high solution quality on a common mortar-based contact treatment with NURBS is additionally observed for the tangential tractions as summarized in Fig. 3. It is noted that while a comparison with approximate analytical solutions is not possible

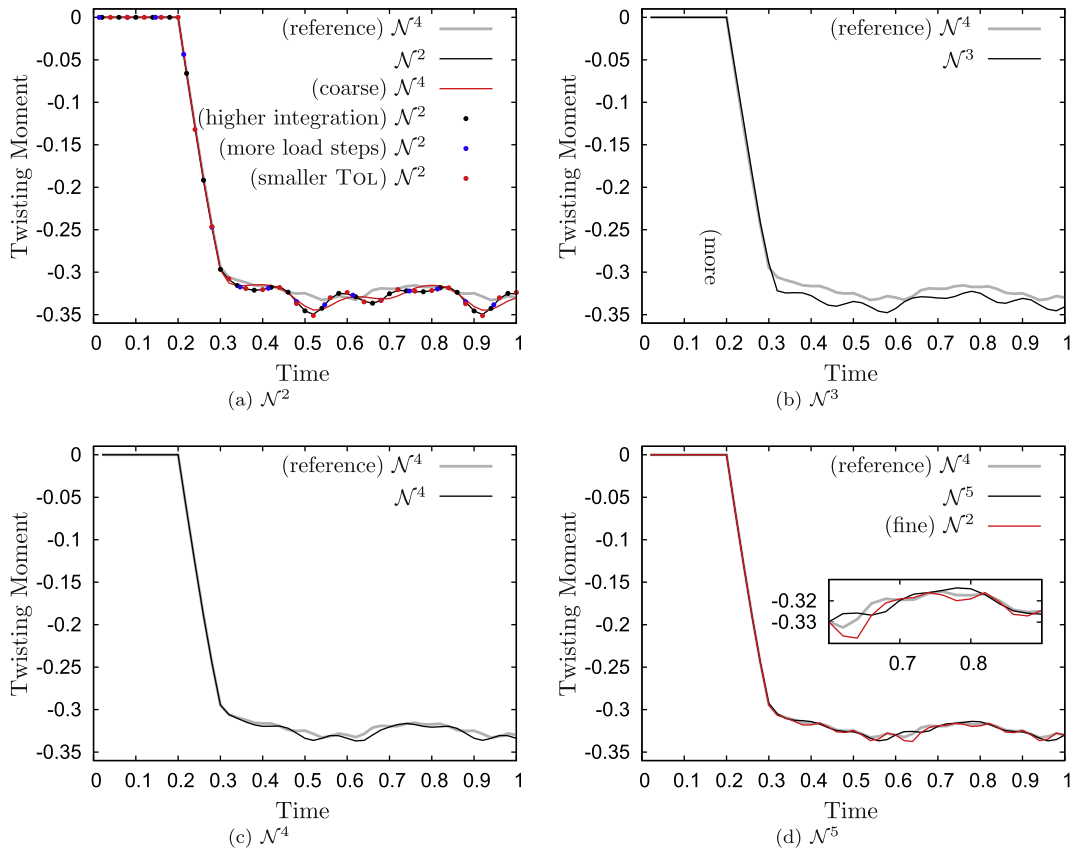

Fig. 6. The results from different $\mathcal{N}^p$-discretizations of Section 4.3 at the standard discretization are compared with a reference $\mathcal{N}^4$ result as well as with alternative choices of numerical parameters.

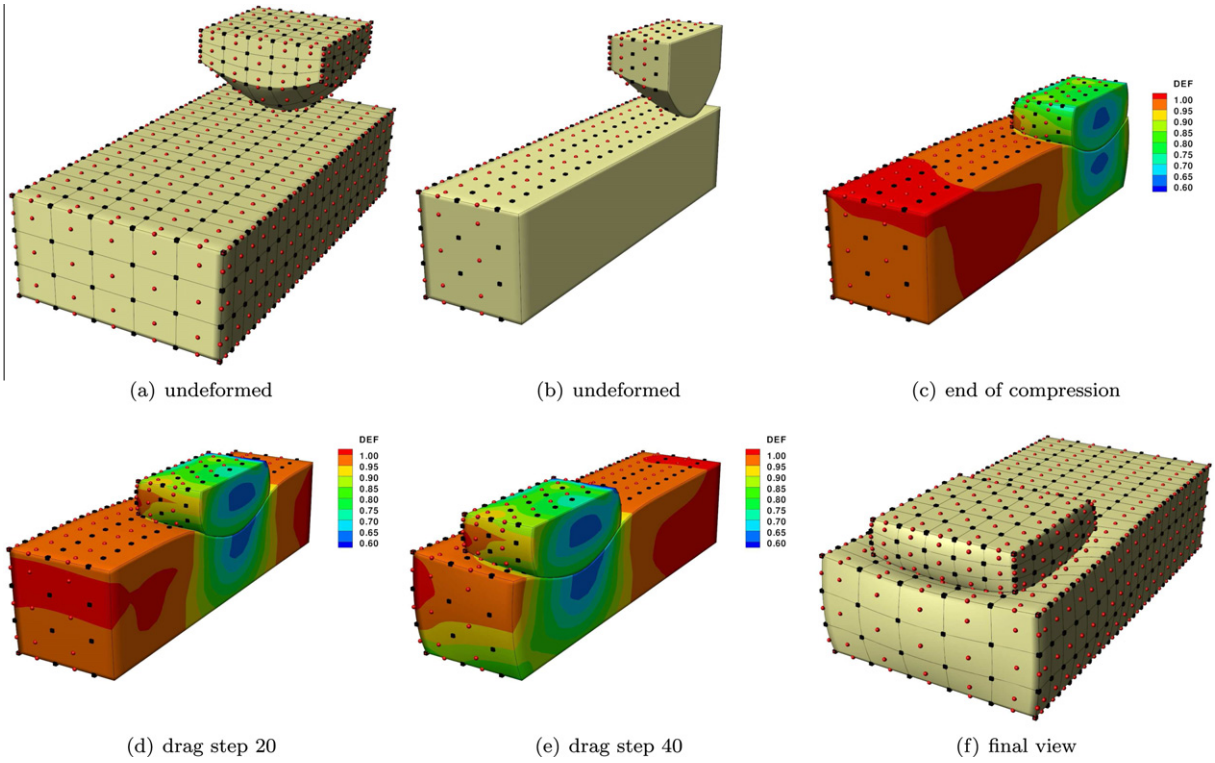

Fig. 7. Simulation instances from the investigation of Section 4.4 are shown at a fine $\mathcal{N}^2$-discretization where large deformations are clearly observed. Here, DEF $\equiv F_{33}$. The lower (master) body has dimensions $3 \times 1.5 \times 0.75$ and the initial gap between the bodies is approximately 0.04 units.

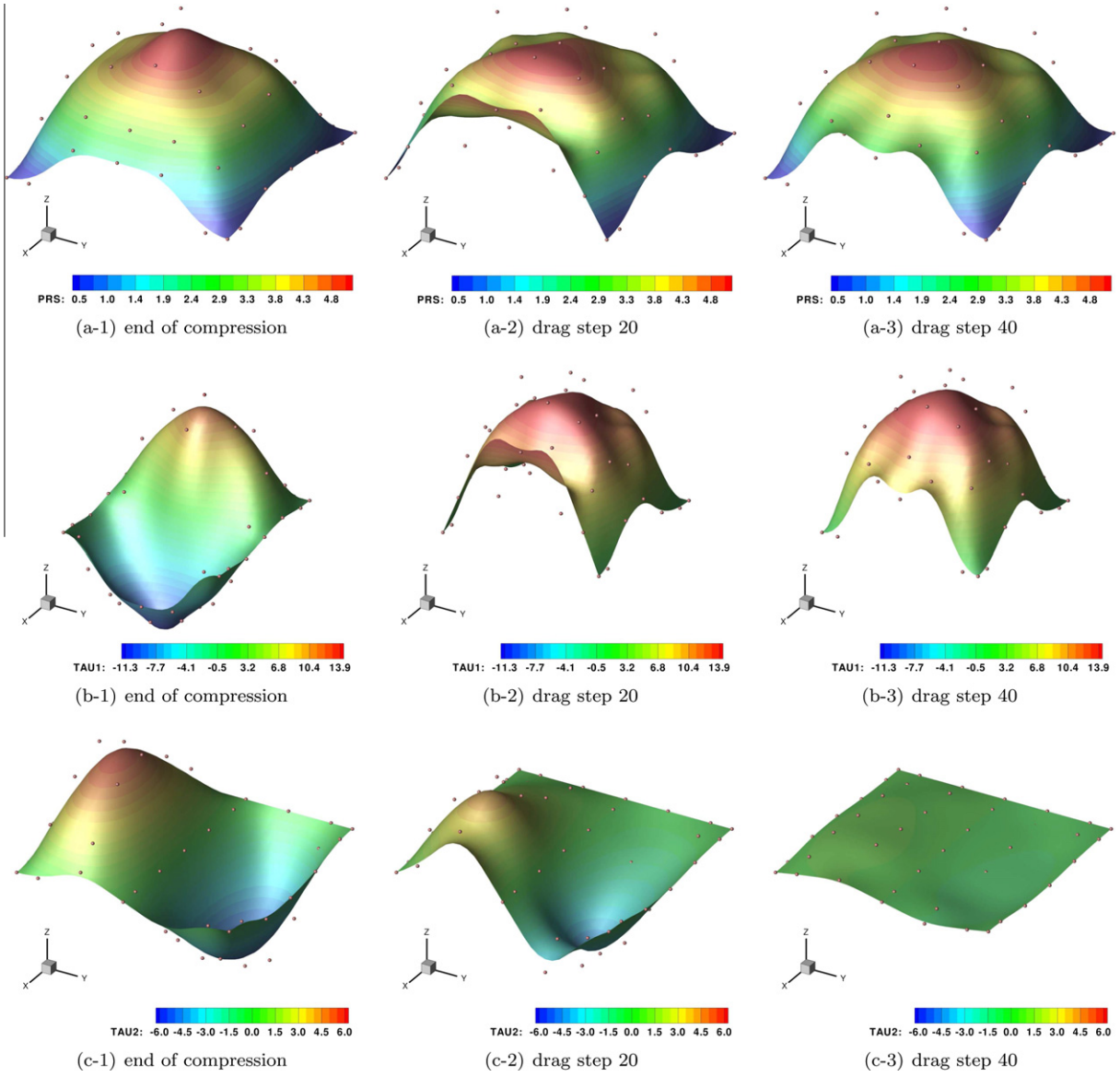

Fig. 8. The contact pressure (PRS $\equiv p_N$) and tangential traction component (TAU1 $\equiv \tau_1/\mu$, TAU2 $\equiv \tau_2/\mu$) evolutions are shown for the analysis of Fig. 7. It is noted that the scaled tangential components can exceed the pressure. This is because the metric components are involved in the mortar projections and only the projected quantities are guaranteed to satisfy the slip criterion.

due to significantly large deformations, the distributions closely resemble the classical results from the analysis of the frictional contact of dissimilar materials under a normal load [23]. Again, $\mathcal{N}^p$ results match the reference solutions accurately whereas a significant deterioration is observed for $\mathcal{L}^{p>1}$. The observation that $\mathcal{L}^1$ is the most robust among all Lagrange discretization on the basis of the present mortar approach will be observed in the upcoming investigations as well. The increase in the number of control points with order elevation has not been addressed here but will be denoted in the following sections where a comparison among different $\mathcal{N}^p$ results will be made.

4.3. Global quality I: twisting moment

In this and the following section, the global quality of the solution is additionally monitored. Presently, the problem setup is summarized in Fig. 4, where half of the geometry is additionally shown to highlight large deformations. The smaller (slave) body top surface is displaced onto the larger (master) body, with equal material properties, in 10 steps of a compression stage through 0.45 units and subsequently rotated through 180° in 40 steps of a twisting stage. In all examples, the master body is held fixed at the bottom surface. While the contact pressure remains approximately constant throughout the twisting stage, the tangential tractions evolve considerably as shown in Fig. 5. The low-valued tractions at the end of the compression stage is due to the fact that the materials are similar. On the other hand, the high tractions and pressures observed at the leading edge during twisting, with respect to rotation, of the contact zone is due to the fold-in tendency that would be more significant at higher friction coefficients. Due to the non-smoothness of Lagrange polynomials, a special modification of the closest-point projection algorithm is required to achieve convergence, in particular at large deformations, such as extending elements beyond their discretization boundaries – see e.g. Laursen [37]. On the other hand, such a treatment is not necessary in the case of NURBS basis functions due to the $\mathcal{C}^1$-continuity of the surface. Consequently, only NURBS discretizations will be employed.

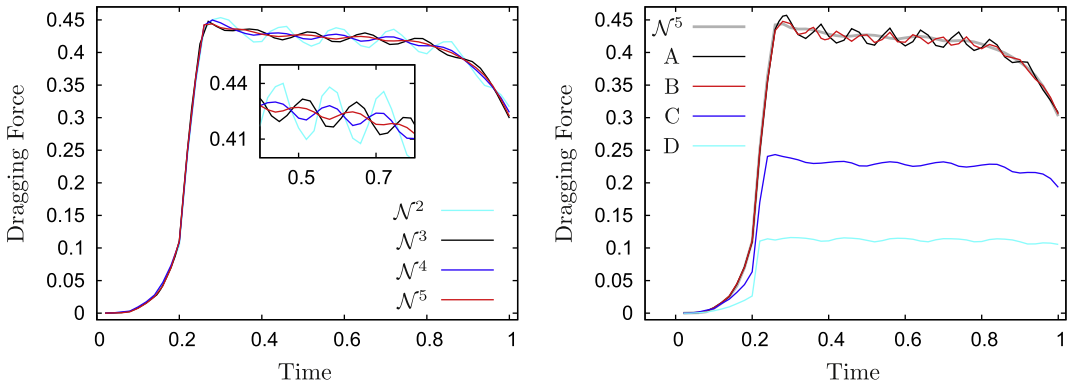

Fig. 9. The results of Section 4.4 are summarized. On the left-hand side, order elevation is carried out, which results in an increase in the number of control points. The effects of smoothness were isolated on the right-hand side, where the $\mathcal{N}^5$ result acts as a reference and the following $\mathcal{N}^2$ cases were considered: (A) 15 master elements along the dragging direction and (B) 20 elements, both having more degrees of freedom than the $\mathcal{N}^5$-discretization, hence highlighting that higher smoothness is advantageous. In investigation (C) 10 elements were used but with the top surface displaced by 0.4 units instead of the standard 0.5 and in (D) by 0.3 units. This is to demonstrate that the response is smoother under lower pressures, however the oscillations remain.

The global solution quality is monitored through the twisting moment applied. The lateral resolution of the master body dictates the solution quality. The slave body in all directions and the vertical direction of the master body are discretized with three $\mathcal{N}^2$ elements while five $\mathcal{N}^p$ elements are employed for each lateral direction of the master, p being a variable. This is the standard discretization. A reference $\mathcal{N}^4$-discretization of the master with eight elements along each lateral direction will be employed for comparison for each choice of p. The results are summarized in Fig. 6. It is noted that the moment will not be a constant due to the comparable size of the master to the slave. The major observation is that the results get smoother and approach the reference solution as p increases. This observation is affected by two factors: (i) increasing $\mathcal{C}^{p-1}$-continuity provided by $\mathcal{N}^p$ basis functions and (ii) increasing number of degrees of freedom through an increase in the number of control points. In order to isolate these effects, the $\mathcal{N}^2$ result is compared with the $\mathcal{N}^4$ one at a coarse discretization with three elements per lateral direction of the master such that both discretizations yield the same number of control points. While the moment evolutions are similar, $\mathcal{N}^4$ delivers a slightly smoother response. This is alternatively observed by comparing the fine $\mathcal{N}^2$-discretization (Fig. 4) result with the standard $\mathcal{N}^5$ response, both with the same number of control points. While both solutions are close to the reference solution, the $\mathcal{N}^2$ result is slightly more oscillatory. This observation demonstrates the advantage of order elevation, which will be further supported and clarified in the next section. Clearly, the possibility of a uniform mortar-based treatment of all orders enables this conclusion.

In closing, it is remarked that alternative choices of the default parameters lead to only negligible changes in the results, as demonstrated in Fig. 6 for $\mathcal{N}^2$. A larger number of contact element integration points (ten instead of six), more load steps (15 normal and 60 tangential) or a smaller augmentation stopping criterion tolerance (TOL = 0.001) are seen to match the default response. Therefore, neither the numerical error in the evaluation of the mortar integrals, nor the integration error associated with the update of the tangential traction components, nor the deviation of the contact tractions from the values of a Lagrange multiplier implementation influence the accuracy or the reliability of the results.

4.4. Global quality II: dragging force

As a second investigation of the global solution quality, the classical ironing example is chosen as shown in Fig. 7 and analyzed again only with $\mathcal{N}^p$-discretizations. The smaller (slave) body top surface is displaced onto the larger (master) body, with equal material properties, through 0.5 units in 10 steps of a compression stage and subsequently moved through the length of the master in 40 steps of a dragging stage through 1.8 units. The friction coefficient is reduced to $\mu = 0.1$ to avoid the physical fold-in effect at the leading contact edge during dragging. The geometry of the slave surface edges is varied with respect to the former example for the same reason, by slightly elevating the corners. The evolutions of p_N and τ_α are shown in Fig. 8 where the high values of p_N and τ_1 are observed near the leading edge, while τ_2 rapidly relaxes to zero during dragging. All distributions are observed to be remarkably smooth even at this relatively coarse discretization.

The global solution quality is monitored through the dragging force applied. The lateral resolution of the master body dictates the solution quality. The dragging direction of the master body is discretized via ten $\mathcal{N}^p$ elements while all other directions are discretized via $\mathcal{N}^2$. The number of elements for the vertical directions are chosen to be three and the lateral directions of the slave and the thickness direction of the master have five elements. The results are summarized in Fig. 9 where the oscillations in the dragging force are easily observed. Clearly, $\mathcal{C}^1$-continuity is not sufficient for a smooth response. Earlier investigations also show that the algorithmic smoothing on $\mathcal{C}^0$-discretizations of the contact interface through a mortar-based approach [49,59] or employing surface smoothing techniques [56,39] do not eliminate these oscillations. This was recently further discussed via a two-dimensional frictional treatment of isogeometric contact analysis in Lorenzis et al. [10]. The source for the oscillations is the strong interaction between the slave body and the boundary layer of the master surface in the vicinity of the contact zone that is significantly deformed. In this strong interaction between the contact and volume discretizations, the master body is able to conform to the deformations imposed by the slave only to the extent of flexibility that is provided by the discretization. This flexibility increases with increasing the continuity to $\mathcal{C}^{p-1}$ with $\mathcal{N}^p$-discretizations. Consequently a smoother force response is expected with increasing p. This is clearly observed in Fig. 9. Here, every other node of intersection for all orders corresponds to where the slave slides out of the span of one master basis function and into another one. A similar interpretation also holds for the earlier example of Section 4.3.

Since increasing p additionally increases the number of control points, in Fig. 9 the reference solution is taken to be $\mathcal{N}^5$ with 770 control points and the $\mathcal{N}^2$-discretization is refined at two stages: the first with 15 elements on the master along the dragging direction (840 control points) and the second with 20 elements (1015

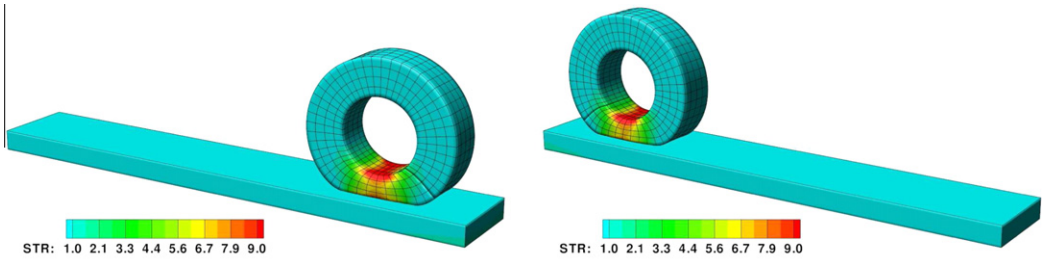

(a) end of compression (b) end of rolling

Fig. 10. Simulation instances from the problem of Section 4.5 with an $\mathcal{N}^2$-discretization ($\mathrm{STR} \equiv \|\boldsymbol{P}\|$). The initial gap between the tire and the surface is zero.

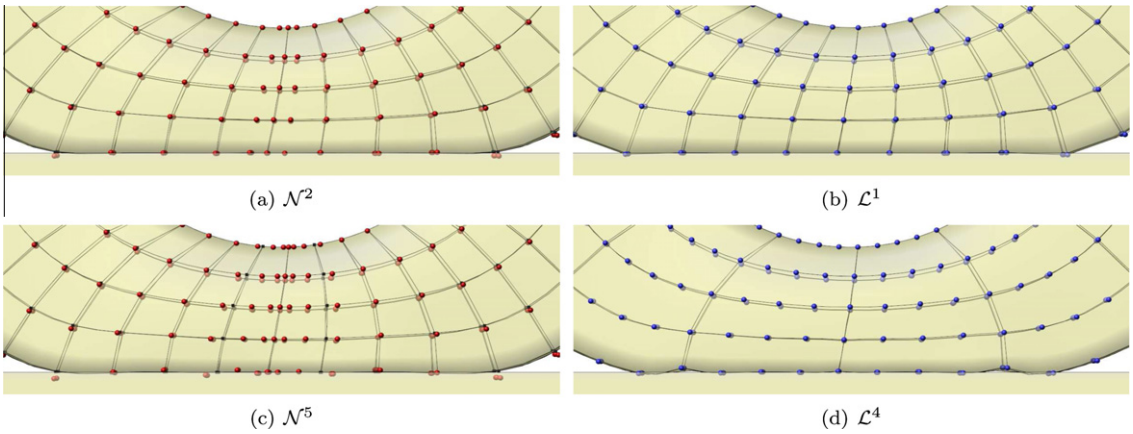

(a) $\mathcal{N}^2$ (b) $\mathcal{L}^1$

(c) $\mathcal{N}^5$ (d) $\mathcal{L}^4$

Fig. 11. A close-up of the contact zone approximately midway through the rolling stage. All bodies are shown as semi-transparent to display the contact interface. It is recalled that the mortar contact constraints do not enforce null gaps for the control points, which is clear in these snapshots.

control points). Although both $\mathcal{N}^2$-discretizations have more degrees of freedom, with the finer resolution oscillations having a larger frequency but a smaller amplitude as expected, the response of the $\mathcal{N}^5$-discretization is clearly significantly smoother. It is noted, as shown in the same figure, that while the magnitude of the oscillations decreases with decreasing normal force, the relative amplitude may be significant. These observations reinforce the observations regarding the advantages of increasing continuity that is possible using NURBS.

4.5. Case study: tire traction

As a last example, an industrially relevant case is investigated by analyzing the rolling motion of a Grosch-wheel by using both $\mathcal{N}^p$- and $\mathcal{L}^p$-discretizations. In all cases, the thickness and width directions are discretized with four $\mathcal{N}^1 \equiv \mathcal{L}^1$ elements while the angular direction discretization is varied. Here, the inner rim of the wheel (undeformed inner/outer radius of 0.25/0.5 units) is compressed onto a rigid track in 10 load steps through a distance of 0.1 units and subsequently rotated through 270° while being displaced horizontally such that the overall motion of the center would correspond to the rolling of a rigid tire about a radius of 0.47 – see Fig. 10.

The friction coefficient is chosen as $\mu = 0.1$ to minimize an effect that is shown in Fig. 11. Since the rotation and displacement do not conform to each other as they would in pure rolling, there is a significant rotation torque applied to the tire which induces ripples through the contact interface at the leading and trailing edges of the contact zone. These are almost non-visible in $\mathcal{N}^p$ discretizations but become amplified for high $\mathcal{L}^p$-discretizations as shown in Fig. 11. As a result, oscillations in the applied torque are monitored as displayed in Fig. 12. The nature, in terms of frequency and magnitude, of these oscillations is similar for all $\mathcal{N}^p$-discretizations and therefore only the $\mathcal{N}^2$ result is shown. The oscillations are again associated with switches in basis function spans, as in Sections 4.3 and 4.4. On the other hand, the magnitude of the oscillations strongly increase with increasing order of Lagrange discretizations although the number of nodes remains constant. However, since order elevation increases the number of control points in the case of NURBS, all $\mathcal{L}^p$-discretizations are redesigned so as to match exactly the number of degrees of freedom for a comparison $\mathcal{N}^{p+1}$ case. Fig. 12 shows that while the $\mathcal{L}^p$ results are now closer to the reference $\mathcal{N}^2$ result in the mean, the oscillations and the deviation from the reference result clearly still increase with increasing Lagrange discretization order. Consequently, while $\mathcal{N}^p$-discretizations deliver a similar or better performance with increasing order on a common mortar-based contact treatment in all examples both at the local and global level, such a common approach does not hold for $\mathcal{L}^p$ discretizations.

It is remarked that in this example the tire rotates through three lines along the thickness direction where only $\mathcal{C}^0$-continuity is ensured due to the initial description of the geometry. However, these points are not discernible in the global torque plots. While a detailed analysis of regions of lower continuity in NURBS discretizations is left as a topic for future investigation, in particular for the case of two deformable bodies, it appears that a small number of such regions does not have significant unfavorable effects. In general, this is an issue where mortar approaches for NURBS may benefit from the algorithmic smoothing ideas that have been developed for mortar-based Lagrange discretizations [49].

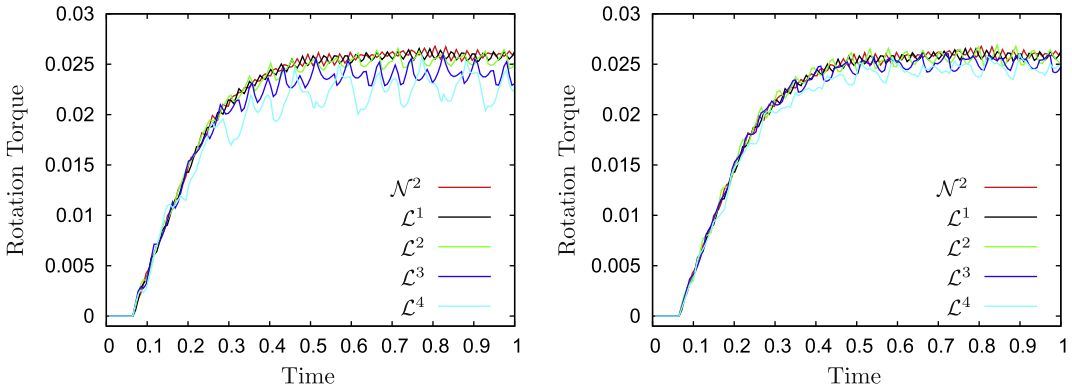

(c-1) Order elevation only (c-2) Order elevation and knot refinement

Fig. 12. The results from the analysis of Fig. 10 are summarized. Since all $\mathcal{N}^p$ results are similar, only the $\mathcal{N}^2$ result is shown. In the left-hand figure, only the discretization order is varied. In the right-hand figure, the number of control points of $\mathcal{L}^p$ discretizations match the number of control points of the $\mathcal{N}^{p+1}$ discretization, in order to isolate order effects (as in Fig. 9). It is remarked that decreasing the augmentation tolerance or increasing the integration order has been tested for $\mathcal{L}^p$ and these have been verified not to influence the results.

5. Conclusion

In order to further address the need for contact treatment in isogeometric analysis with NURBS, a three-dimensional frictional mortar-based approach was presented as an extension to recent work on two- and three-dimensional frictionless thermomechanical contact [58] and two-dimensional frictional contact [10]. The central ingredient of the mortar-based approach is the enforcement of the contact constraints through projections to control point quantities in order to avoid a potentially under- or overconstrained formulation.

It was demonstrated that the presented approach delivers robust local results even at coarse resolutions of the contact interface with smooth pressure and tangential traction distributions. In particular, the pressure distribution is guaranteed to be non-negative and the traction distributions remain minimally oscillatory with respect to alternative Lagrange discretizations. These observations reinforce the advantageous result that *the presented mortar-based approach serves as a common basis for treating isogeometric contact analysis problems with varying orders of discretization throughout the contact surface and the volume*. Conversely, the same common basis does not appear to deliver satisfactory results for Lagrange discretizations, which display an increasingly oscillatory behavior with higher orders, in particular at coarse resolutions.

At the global level, convergence problems associated with the closest-point projection algorithm of contact are naturally avoided due to the guaranteed $\mathcal{C}^1$-continuity of the NURBS-based contact surface description that is inherited directly from the volume description in various standard benchmark problems of computational contact mechanics. Additionally, the advantage of order elevation was demonstrated where increasing continuity leads to smoother evolutions of sample global measures, such as the applied tangential force or the twisting moment. In problems governed by strong interactions between the contact and volume discretizations, $\mathcal{C}^1$-continuity alone is not sufficient and higher-order continuity is needed to allow the deforming bodies to better conform to each other's geometry. The present capabilities may also help alleviate the oscillatory response in closely related interface mechanics problems such as peeling computations [51].

From a design point of view, a single NURBS patch or a simple combination of multiple NURBS patches may not describe a geometry accurately or may do so in a nonoptimal fashion with an initially high number of control points. From an analysis point of view, accuracy of the contact response at the local and/or global level is strongly governed by the boundary layers of the deformable bodies in the vicinity of the contact zone only and hence it is not numerically favorable to refine the geometry in regions away from this zone as well. Both of these cases call for the ability of locally controlled knot refinement and order elevation. Such a framework is provided through T-splines as remarked in the introduction. Ongoing research in this area is delivering novel technologies that have potential application in the efficient and reliable treatment of contact problems on a common basis. Such capabilities may also help further improve the traction distributions by resolving the edge of the contact zone [15].

References

[1] F. Aurrichio, L. Beiraõ Da Veiga, T.J.R. Hughes, A. Reali, G. Sangalli, Isogeometric collocation methods, Math. Models Methods Appl. Sci. 20 (2010) 2075–2107.
[2] Y. Bazilevs, I. Akkerman, Large eddy simulation of turbulent Taylor–Couette flow using isogeometric analysis and the residual-based variational multiscale method, J. Comput. Phys. 229 (2010) 3402–3414.
[3] Y. Bazilevs, C. Michler, V.M. Calo, T.J.R. Hughes, Isogeometric variational multiscale modeling of wall-bounded turbulent flows with weakly enforced boundary conditions on unstretched meshes, Comput. Methods Appl. Mech. Engrg. 199 (2010) 780–790.
[4] D.J. Benson, Y. Bazilevs, M.-C. Hsu, T.J.R. Hughes, A large deformation rotation-free, isogeometric shell, Int. J. Numer. Methods Engrg. 200 (2011) 1367–1878.
[5] D.J. Benson, Y. Bazilevs, E.D. Luycker, M.-C. Hsu, M. Scott, T.J.R. Hughes, T. Belytschko, A generalized finite element formulation for arbitrary basis functions: from isogeometric analysis to XFEM, Int. J. Numer. Methods Engrg. 83 (2010) 765–785.
[6] J. Berkley, G. Turkiyyah, D. Berg, M. Ganter, S. Weghorst, Real-time finite element modeling for surgery simulation: an application to virtual suturing, IEEE Trans. Visualiz. Comput. Graph. 10 (2004) 314–325.
[7] M.J. Borden, C.V. Verhoosel, M.A. Scott , T.J.R. Hughes, C.M. Landis, A phase-field description of dynamic brittle fracture, Comput. Methods Appl. Mech. Engrg., submitted for publication.
[8] A. Buffa, G. Sangalli, R. Vazquez, Isogeometric analysis in electromagnetics: B-splines approximation, Comput. Methods Appl. Mech. Engrg. 199 (2010) 1143–1152.
[9] J.A. Cottrell, T.J.R. Hughes, Y. Bazilevs, Isogeometric Analysis, Wiley, 2009.
[10] L. De Lorenzis, İ. Temizer, P. Wriggers, G. Zavarise, A large deformation frictional contact formulation using NURBS-based isogeometric analysis, Int. J. Numer. Methods. Engrg. (2011). online – doi:10.1002/nme.3159.
[11] M.R. Dörfel, B. Jüttler, B. Simeon, Adaptive isogeometric analysis by local h-refinement with T-splines, Comput. Methods Appl. Mech. Engrg. 199 (2010) 264–275.
[12] A.L. Eterovic, K.J. Bathe, An interface interpolation scheme for quadratic convergence in the finite element analysis of contact problems, Computational Methods in Nonlinear Mechanics, Springer-Verlag, Berlin, New York, 1991, pp. 703–715.
[13] K.A. Fischer, P. Wriggers, Frictionless 2D contact formulations for finite deformations based on the mortar method, Comput. Mech. 36 (2005) 226–244.
[14] K.A. Fischer, P. Wriggers, Mortar based frictional contact formulation for higher order interpolations using the moving friction cone, Comput. Methods Appl. Mech. Engrg. 195 (2006) 5020–5036.

[15] D. Franke, A. Düster, V. Nübel, E. Rank, A comparison of the *h*-, *p*-, *hp*-, and *rp*-version of the FEM for the solution of the 2D Hertzian contact problem, Comput. Mech. 45 (2010) 513–522.
[16] H. Gomez, V.M. Calo, Y. Bazilevs, T.J.R. Hughes, Isogeometric analysis of the Cahn–Hilliard phase-field model, Comput. Methods Appl. Mech. Engrg. 197 (2008) 4333–4352.
[17] H. Gomez, T.J.R. Hughes, X. Nogueira, V.M. Calo, Isogeometric analysis of the isothermal Navier–Stokes–Korteweg equations, Comput. Methods Appl. Mech. Engrg. 199 (2010) 1828–1840.
[18] E. Hansson, A. Klarbring, Rigid contact modelled by CAD surface, Engrg. Comput. 7 (1990) 344–348.
[19] J.-H. Heegaard, A. Curnier, An augmented Lagrange method for discrete large-slip contact problems, Int. J. Numer. Methods Engrg. 36 (1993) 569–593.
[20] A. Heege, P. Alart, A frictional contact element for strongly curved contact problems, Int. J. Numer. Methods Engrg. 39 (1996) 165–184.
[21] C. Hesch, P. Betsch, A mortar method for energy-momentum conserving schemes in frictionless dynamic contact problems, Int. J. Numer. Meth. Engrg. 77 (2009) 1468–1500.
[22] P. Hild, Numerical implementation of two nonconforming finite element methods for unilateral contact, Comput. Methods Appl. Mech. Engrg. 184 (2000) 99–123.
[23] D.A. Hills, D. Nowell, A. Sackfield, Mechanics of Elastic Contacts, Butterworth Heinemann, Oxford, 1993.
[24] S. Hüeber, M. Mair, B.I. Wohlmuth, A priori error estimates and an inexact primal–dual active set strategy for linear and quadratic finite elements applied to multibody contact problems, Appl. Numer. Math. 54 (2005) 555576.
[25] S. Hüeber, B.I. Wohlmuth, A primal-dual active set strategy for non-linear multibody contact problems, Comput. Methods Appl. Mech. Engrg. 194 (2005) 3147–3166.
[26] S. Hüeber, B.I. Wohlmuth, Thermo-mechanical contact problems on non-matching meshes, Comput. Methods Appl. Mech. Engrg. 198 (2009) 1338–1350.
[27] T.J.R. Hughes, J.A. Cottrell, Y. Bazilevs, Isogeometric analysis: CAD, finite elements, NURBS, exact geometry and mesh refinement, Comput. Methods Appl. Mech. Engrg. 194 (2005) 4135–4195.
[28] T.J.R. Hughes, A. Reali, G. Sangalli, Efficient quadrature for NURBS-based isogeometric analysis, Comput. Methods Appl. Mech. Engrg. 199 (2010) 301–313.
[29] R.W. Johnson, Higher order B-spline collocation at the Greville abscissae, Appl. Numer. Math. 52 (2005) 63–75.
[30] R.E. Jones, P. Papadopoulos, A novel three-dimensional contact finite element based on smooth pressure interpolations, Int. J. Numer. Methods. Engrg. 51 (2001) 791–811.
[31] J. Kiendl, K. Bletzinger, J. Linhard, R. Wüchner, Isogeometric shell analysis with Kirchhoff–Love elements, Comput. Methods Appl. Mech. Engrg. 198 (2009) 3902–3914.
[32] A. Konyukhov, K. Schweizerhof, Incorporation of contact for high-order finite elements in covariant form, Comput. Methods Appl. Mech. Engrg. 198 (2009) 12131223.
[33] A. Konyukhov, K. Schweizerhof, Geometrically exact covariant approach for contact between curves, Comput. Methods Appl. Mech. Engrg. 199 (2010) 2510–2531.
[34] A. Konyukhov, K. Schweizerhof, Geometrically exact theory for contact interactions of 1D manifolds. Algorithmic implementation with various finite element models, Comput. Methods Appl. Mech. Engrg. 205–208C (2012) 130–138.
[35] L. Krstulovic-Opara, P. Wriggers, J. Korelc, A C^1-continuous formulation for 3D finite deformation frictional contact, Computational Mechanics 29 (2002) 27–42.
[36] R.L. Landon, M.W. Hast, S.J. Piazza, Robust contact modeling using trimmed nurbs surfaces for dynamic simulations of articular contact, Comput. Methods Appl. Mech. Engrg. 198 (2009) 23392346.
[37] T.A. Laursen, Computational Contact and Impact Mechanics, 1st ed., Springer, Berlin Heidelberg New York, 2003. corr. 2nd printing.
[38] T.A. Laursen, M.A. Puso, J. Sanders, Mortar contact formulations for deformabledeformable contact: past contributions and new extensions for enriched and embedded interface formulations, Comput. Methods Appl. Mech. Engrg. 205–208C (2012) 3–15.
[39] J. Lengiewicz, J. Korelc, S. Stupkiewicz, Automation of finite element formulations for large deformation contact problems, International Journal for Numerical Methods in Engineering 85 (2011) 1252–1279.
[40] J. Lu, Isogeometric contact analysis: Geometric basis and formulation of frictionless contact, Comput. Methods Appl. Mech. Engrg. 200:726 (2011) 741.
[41] D.D. Nelson, E. Cohen, Optimization-based virtual surface contact manipulation at force control rates, in: VR '00 Proceedings of the IEEE Virtual Reality 2000 Conference, 2000, p.37.
[42] V. Padmanabhan, T.A. Laursen, A framework for development of surface smoothing procedures in large deformation frictional contact analysis, Finite Elements in Analysis and Design 37 (2001) 173–198.
[43] J.M.S.P. Papadopoulos, An analysis of dual formulations for the finite element solution of two-body contact problems, Computer Methods in Applied Mechanics and Engineering 194 (2005) 27342780.
[44] P. Papadopoulos, J.M. Solberg, A Lagrange multiplier method for the finite element solution of frictionless contact problems, Math. Comput. Model. 28 (1998) 373–384.
[45] L. Piegl, W. Tiller, The NURBS Book, 2nd ed., Springer, Berlin Heidelberg New York, 1996.
[46] G. Pietrzak, A. Curnier, Large deformation frictional contact mechanics: continuum formulation and augmented Lagrangean treatment, Computer Methods in Applied Mechanics and Engineering 177 (1999) 351–381.
[47] C. Politis, A.I. Ginnis, P.D. Kaklis, K. Belibassakis, C. Feurer, An isogeometric BEM for exterior potential-flow problems in the plane, in: 2009 SIAM/ACM Joint Conference on Geometric and Physical Modeling (SPM 09), San Francisco, CA, 2009, pp. 349–354.
[48] A. Popp, M.W. Gee, W.A. Wall, A finite deformation mortar contact formulation using a primal-dual active set strategy, Int. J. Numer. Meth. Engng. 79 (2009) 1354–1391.
[49] M.A. Puso, T.A. Laursen, A mortar segment-to-segment frictional contact method for large deformations, Comput. Methods Appl. Mech. Engrg. 193 (2004) 4891–4913.
[50] M.A. Puso, T.A. Laursen, J. Solberg, A segment-to-segment mortar contact method for quadratic elements and large deformations, Comput. Methods Appl. Mech. Engrg. 197 (2008) 555–566.
[51] R.A. Sauer, Enriched contact finite elements for stable peeling computations, International Journal for Numerical Methods in Engineering 87 (2011) 593–616.
[52] M.A. Scott, M.J. Borden, C.V. Verhoosel, T.W. Sederberg, T.J.R. Hughes, Isogeometric finite element data structures based on Bézier extraction of T-splines, Int. J. Numer. Meth. Engrg. (2011). online – doi: 10.1002/nme.3167.
[53] M.A. Scott, X. Li, T.W. Sederberg, T.J.R. Hughes, Local refinement of analysis-suitable T-splines, Comput. Methods Appl. Mech. Engrg., submitted for publication.
[54] J.C. Simo, P. Wriggers, R.L. Taylor, A perturbed lagrangian formulation for the finite element solution of contact problems, Comput. Methods Appl. Mech. Engrg. 50 (1985) 163–180.
[55] J.M. Solberg, R.E. Jones, P. Papadopoulos, A family of simple two-pass dual formulations for the finite element solution of contact problems, Computer Methods in Applied Mechanics and Engineering 196 (2007) 782–802.
[56] M. Stadler, G.A. Holzapfel, J. Korelc, C^n continuous modelling of smooth contact surfaces using NURBS and application to 2D problems, Int. J. Numer. Meth. Engng. 57 (2003) 2177–2203.
[57] İ. Temizer, A mixed formulation of mortar-based frictionless contact, Comput. Methods Appl. Mech. Engrg., submitted for publication.
[58] İ. Temizer, P. Wriggers, T.J.R. Hughes, Contact treatment in isogeometric analysis with NURBS, Comput. Methods Appl. Mech. Engrg. 200 (2011) 1100–1112.
[59] M. Tur, F.J. Fuenmayor, P. Wriggers, A mortar-based frictional contact formulation for large deformations using Lagrange multipliers, Comput. Methods Appl. Mech. Engrg. 198 (2009) 2860–2873.
[60] P. Wriggers, Computational Contact Mechanics, 2nd ed., Springer, Berlin Heidelberg New York, 2006.
[61] P. Wriggers, M. Imhof, On the treatment of nonlinear unilateral contact problems, Archive of Applied Mechanics 63 (1993) 116–129.
[62] P. Wriggers, L. Krstulovic-Opara, J. Korelc, Smooth C^1- interpolations for two-dimensional frictional contact problems, International Journal for Numerical Methods in Engineering 51 (2001) 1469–1495.
[63] G. Zavarise L. De Lorenzis R.L. Taylor, A non-consistent start-up procedure for contact problems with large load-steps, Comput. Methods Appl. Mech. Engrg. 205–208C (2012) 91–109.